Ionic Conductances of Squid Giant Fiber Lobe Neurons

ISABEL LLANO and RICHARD J. BOOKMAN

From the Department of Physiology, University of Pennsylvania, Philadelphia, Pennsylvania 19104, and the Marine Biological Laboratory, Woods Hole, Massachusetts 02543

ABSTRACT The cell bodies of the neurons in the giant fiber lobe (GFL) of the squid stellate ganglion give rise to axons that fuse and thereby form the third-order giant axon, whose initial portion functions as the postsynaptic element of the squid giant synapse. We have developed a preparation of dissociated, cultured cells from this lobe and have studied the voltage-dependent conductances using patch-clamp techniques. This system offers a unique opportunity for comparing the properties and regional differentiation of ionic channels in somatic and axonal membranes within the same cell. Some of these cells contain a small inward Na current which resembles that found in axon with respect to tetrodotoxin sensitivity, voltage dependence, and inactivation. More prominent is a macroscopic inward current, carried by Ca^{2+}, which is likely to be the result of at least two kinetically distinct types of channels. These Ca channels differ in their closing kinetics, voltage range and time course of activation, and the extent to which their conductance inactivates. The dominant current in these GFL neurons is outward and is carried by K^+. It can be accounted for by a single type of voltage-dependent channel. This conductance resembles the K conductance of the axon, except that it partially inactivates during relatively short depolarizations. Ensemble fluctuation analysis of K currents obtained from excised outside-out patches is consistent with a single type of K channel and yields estimates for the single channel conductance of ~13 pS, independently of membrane potential. A preliminary analysis of single channel data supports the conclusion that there is a single type of voltage-dependent, inactivating K channel in the GFL neurons.

INTRODUCTION

The third-order giant axon of the squid arises from the complete fusion of hundreds of individual axons of neurons located in the stellate ganglion. This morphological arrangement for achieving a large axonal diameter in order to increase the nerve impulse conduction velocity was originally described by Young (1939). All of the cell bodies whose axons fuse to form the third-order giant axon are segregated in a part of the stellate ganglion that Young called the giant

Address reprint requests to Dr. Isabel Llano, Laboratoire de Neurobiologie, Ecole Normale Supérieure, 46 rue d'Ulm, 75005 Paris, France. Dr. Bookman's present address is Biozentrum, University of Basel, Basel CH-4056, Switzerland.

J. GEN. PHYSIOL. © The Rockefeller University Press · 0022-1295/86/10/0543/27$1.00

Volume 88 October 1986 543–569

fiber lobe (GFL). His anatomical description called attention to the virtues of this axonal preparation for the study of the ionic basis of the action potential and the development of voltage-clamp techniques in the study of excitable membranes (Cole, 1949; Marmont, 1949; Hodgkin et al., 1952).

Electrophysiological evidence corroborating the syncytial origin of the squid giant axon was provided by Miledi (1967), who reported that action potentials produced in the giant axon were propagated electrotonically to many cells in the GFL. Miledi's study further suggested that the voltage-dependent ionic channels of GFL cells may differ significantly in their functional properties or relative densities from those of the axonal membrane, since GFL cells are not capable of sustaining action potentials.

Because of their unique anatomical arrangement, the GFL and the postganglionic giant axon to which its cells give rise offer an excellent opportunity to perform a comparative study of the properties of ionic channels in two spatially segregated areas of the same cell (i.e., its soma and axonal process). We have developed a method for the isolation, dissociation, and culturing of these GFL neurons in order to address a number of questions. This article describes the voltage-dependent ionic conductances that we have observed in these molluscan somata through the use of both the whole cell and the excised patch configuration of the patch-clamp technique (Hamill et al., 1981), and compares our findings with some of the data from axonal recordings. Some of our results have been presented in abstract form (Llano and Bookman, 1985; Bookman et al., 1985).

METHODS

Preparation

Squid (*Loligo pealei*) with a mantle length of ~10 cm were used. Following standard procedures for the gross dissection of the squid, the viscera were removed and the mantle was pinned out flat to expose the stellate ganglia and the stellar nerves. After the (postsynaptic) third-order giant axon was tied off and the other stellar nerves were cut, the stellate ganglion was lifted from the mantle and transferred to a dish where the connective tissue capsule surrounding the GFL was dissected out. Our choice of squid smaller than those used for axonal experiments was based on the relative ease of this part of the procedure as well as the smaller size of the resulting cell bodies (see below). The lobe was cut away from the rest of the ganglion and placed in a petri dish containing artificial seawater (ASW) (Table I) to which 10 mg/ml of protease (type XIV, Sigma Chemical Co., St. Louis, MO) had been added. After 40–60 min of incubation at room temperature, the tissue was placed in a plastic 1-ml Eppendorf tube filled with sterile, filtered ASW and then washed several times to remove any remaining enzyme. The tube was held in a vortexer for 30–60 s in order to disperse the cells mechanically. The resulting suspension of cells was transferred to tissue culture dishes (Primaria, Falcon Labware, Becton, Dickinson & Co., Oxnard, CA) or slivers of glass coverslips by means of fire-polished Pasteur pipettes. Glass coverslips were cleaned (xylene, acetone, and ethanol washes for ~15 min each) and treated with poly-L-lysine (1 mg/ml dissolved in 0.15 M Trizma, pH 8.5) for 16 h. Usually, cells adhered to the bottom of the culture dishes or coverslips within 30 min. The slips offered the advantage over round dishes of permitting the use of an experimental chamber with a small volume (~0.5 ml), in which the exchange of solutions and the control of temperature were efficiently achieved.

For the work presented in this article, we used acutely dissociated cells (i.e., a few hours after plating) as well as cells maintained in culture for up to 15 d. For the latter, a culture medium similar to that previously described for the culture of *Aplysia* neurons (Dagan and Levitan, 1981) was used. The composition was: 50% Leibovitz-15 tissue culture medium (320-1415, Gibco Laboratories, Grand Island, NY) and 50% of a stock salt solution containing 780 mM NaCl, 14.2 mM KCl, 108 mM $MgCl_2$, and 21 mM $CaCl_2$. This was supplemented with 4% fetal calf serum (FBS-309, Gibco Laboratories), 2.5 mg/ml glucose, 1 mM L-glutamine (320-5030, Gibco Laboratories), and 100 U/ml penicillin-streptomycin (600-5140, Gibco Laboratories). The cells were kept in an incubator at 10–15°C, and were viable for at least 3 wk.

The dissociation procedure described above yielded a large number of intact neuronal cell bodies ranging in diameter from 15 to 70 μm (Fig. 1*A*). Some of these cell bodies had roughly spherical shapes and no processes, whereas others had retained a portion of their

TABLE I

Recording Solutions

		Concentration
		mM
ASW	NaCl	440
	KCl	5
	$CaCl_2$	10
	$MgCl_2$	50
	HEPES	10
KFG	K-glutamate	250
	K-fluoride	25
	KCl	20
	Sucrose	400
	HEPES	10
	EGTA	10
NMG	NMG-glutamate	225
	NMG-fluoride	25
	TEA-Cl	25
	Sucrose	400
	HEPES	10
	EGTA	10

axons. In addition, we often saw what appeared to be elongated fragments of axon resting on the bottom of the dish. The higher-power views in Fig. 1*B* show examples of the types of cells obtained. Some of these have flattened out processes with flaring ends that resemble growth cones, with long protruding microspikes.

Experimental Procedures

To maximize the quality of spatial control of membrane potential, experiments were done on round cells, 20–40 μm in diameter, which had no axonal stump, e.g., the cells indicated by the arrows in Fig. 1*B*. The temperature in the chamber was maintained at 10–12°C by means of a Peltier unit. A list of the solutions used is given in Table I. The osmolality of all solutions was adjusted to 990 mosmol for internal solutions and 1,000–1,010 mosmol for external solutions; they were buffered to a pH of 7.3.

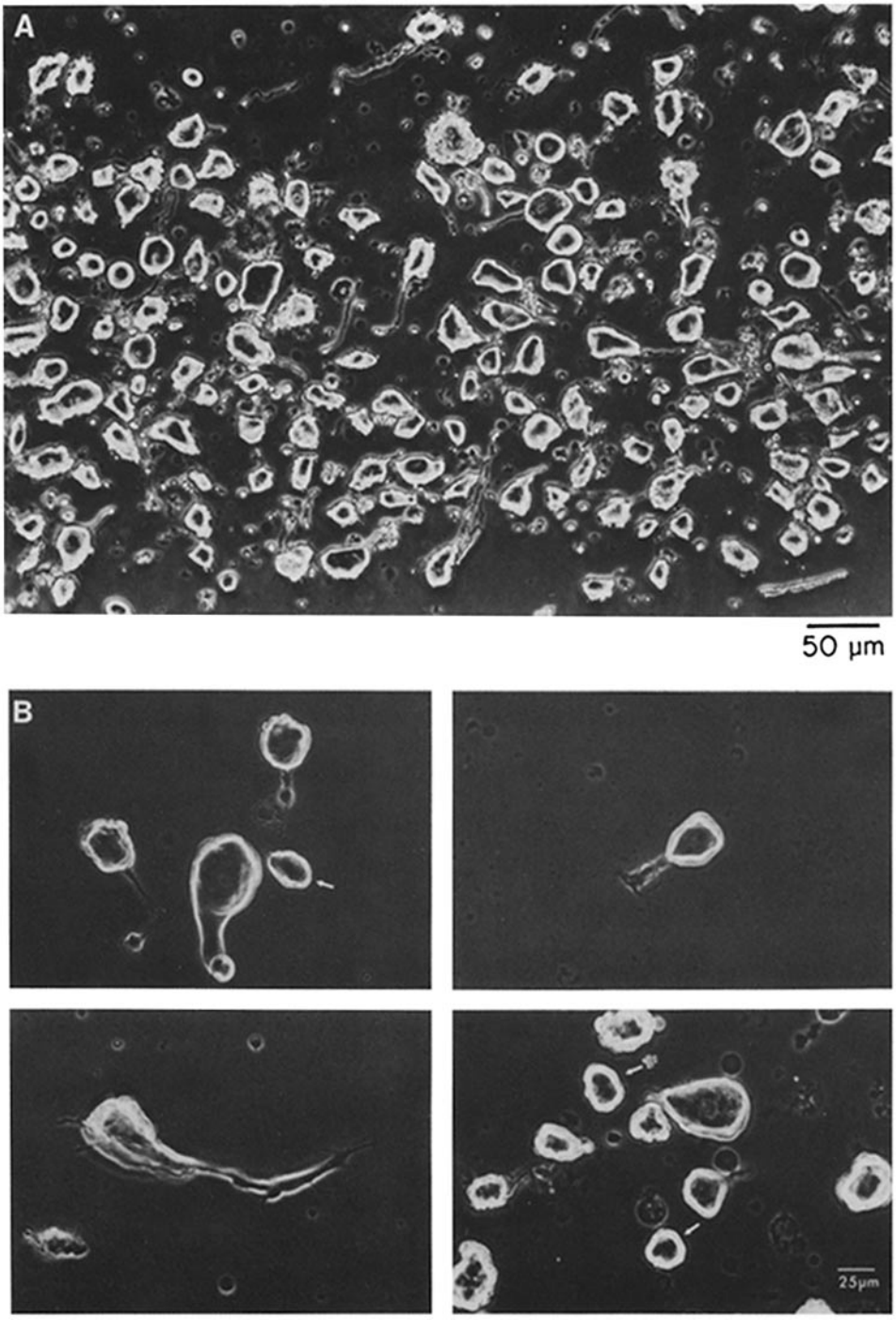

FIGURE 1. Typical cells obtained after dissociation of the squid giant fiber lobe. See text for details.

Recordings of whole cell currents were obtained using patch pipettes made from Corning glass 8161 (recommended to us by Dr. Jim Rae), having resistances of 450 kΩ to 1.2 MΩ when filled with the standard K solution (KFG, Table I), and coated with Sylgard (type 184, Dow Chemical Co., Midland, MI) to minimize capacitance. The pipettes were connected via an Ag/AgCl wire to a current-to-voltage converter that followed the design of Sigworth (1983) but had a low feedback resistance (100 MΩ). The later stages of the amplifier had provisions for applying DC potential changes and compensating for both series resistance and pipette/membrane capacitance. To null junction potentials, the current measured through the pipette in the bath, before seal formation, was adjusted to zero via the DC command potential control. The amount of resistance in series with the membrane was estimated by the change in the capacity transient upon breaking into the cell according to the procedure described by Matteson and Armstrong (1984*a*). We have found that this quantity was usually two to three times the initial pipette resistance and that almost all of it could be compensated for electronically. This compensation was usually applied empirically after breaking into the cells and checked several times during the course of an experiment. Current records were filtered with a six-pole Bessel filter at a corner frequency of 10 kHz. The P/2 procedure (Armstrong and Bezanilla, 1974) was used to subtract the linear components of the leakage and capacitive currents and it was always applied from a subholding potential of −130 mV, regardless of the holding potential used.

For the recording of currents in the excised patch configuration, we used Sylgard-coated pipettes with higher resistances (2–7 MΩ), made from either Corning glass 7052 or 8161. The current-to-voltage converter used was of the same design but with a feedback resistance of 10 GΩ. A single-stage, high-frequency booster was used to compensate for the frequency response of the converter (Sigworth, 1983). Our initial implementation of this high-gain amplifier had a bandwidth of 2.5–3.0 kHz, which was later improved to extend the frequency response out to ~7.5 kHz. The current traces were filtered with a six-pole Bessel filter at a corner frequency of 5 kHz.

Data were acquired, stored, and analyzed with an LSI-11/23 computer (Digital Equipment Corp., Maynard, MA) interfaced to the analog electronics through a system, designed in this laboratory, used for pulse generation, data acquisition, and display.

RESULTS

General Observations

The total membrane currents were recorded with K-containing pipettes (KFG, Table I) under whole-cell voltage clamp from neurons bathed in ASW (Fig. 2*A*). When the membrane voltage was stepped from a holding potential (HP) of −90 mV to the values indicated near each trace, large outward currents were observed that approached their steady state in 10–15 ms. These currents were not significantly blocked by the external application of either 4-aminopyridine (in concentrations of up to 2 mM) or tetraethylammonium (TEA) (in concentrations of up to 40 mM). However, they were completely eliminated by replacement of the internal K^+ by the impermeant cation *N*-methyl-*d*-glucamine (NMG) and addition of TEA to the internal solution. Under these ionic conditions (NMG, Table I), 10-ms depolarizations from a holding potential of −90 mV elicited currents that were inward in direction (Fig. 2*B*) and much smaller than those recorded with K-containing pipettes; they were often masked by the outward currents if K^+ was in the pipette.

Inward Currents

The inward current shown in Fig. 2*B* had at least two components that can be distinguished in several ways. Fig. 3 shows the currents recorded during a 20-ms depolarization to −10 mV from a holding potential of −90 mV before (upper

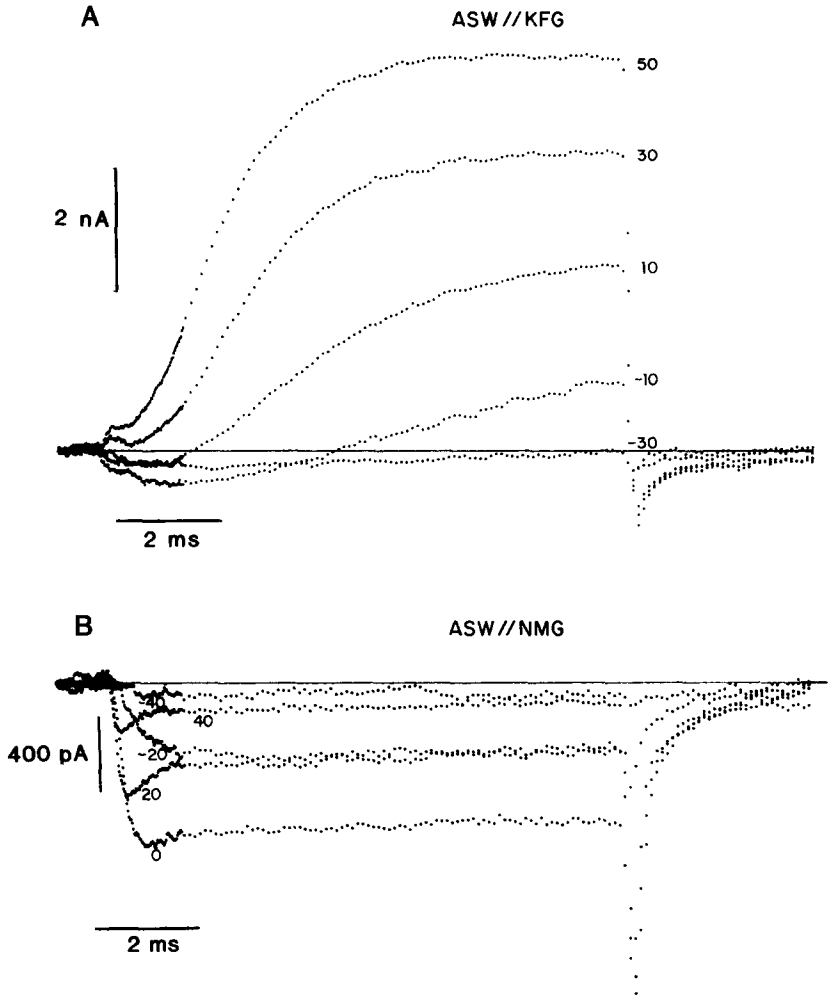

FIGURE 2. Ionic currents recorded from GFL neurons during 10-ms voltage-clamp pulses, in the presence (*A*) and absence (*B*) of internal K^+. Holding potential, −90 mV; depolarizing steps were applied to the values indicated in front of each trace. The P/2 procedure was used in this and all other records presented.

trace) and after (middle trace) the addition of 200 nM tetrodotoxin (TTX) to the bathing solution. The addition of TTX eliminates a fast-activating component, although it has little effect on either the maintained level of current during the pulse or the current at the OFF of the pulse. The difference record, or TTX-

sensitive component (lower trace), activated fairly rapidly, reaching its peak in ~1.7 ms for this pulse to −10 mV, and declined to a low steady state level at the end of the 20-ms pulse with a time constant of 2.7 ms.

The TTX-sensitive component of the inward current (I_{Na}) varies widely in magnitude from preparation to preparation and usually comprises a small fraction of the total inward current. Fig. 4 shows the effect of a prepulse on a cell with a large I_{Na} to illustrate that it can also be eliminated through the use of depolarizing prepulses. The upper traces show currents recorded during depolarizations to 0 mV after 25-ms prepulses to various potentials. Both the peak

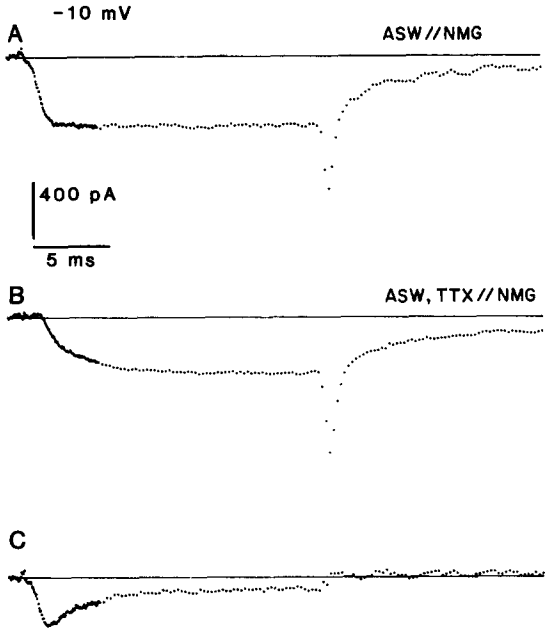

FIGURE 3. Effect of TTX on the inward current. Currents were recorded at −10 mV from cells bathed in ASW without (*A*) and with (*B*) 200 nM TTX. Internal solution, NMG. Holding potential, −90 mV. (*C*) TTX-sensitive component of the inward current obtained by subtracting the record in *B* from that in *A*.

and steady state values of the inward current declined as the magnitude of the prepulse was increased. The lower part of Fig. 4 shows a plot of the normalized peak current amplitude during the test pulse as a function of the membrane voltage during the preceding pulse. This steady state inactivation curve has a midpoint at −45 mV and saturates at approximately −20 mV at a level of ~10%.

Although we have not made a detailed study of its properties, it is clear that this component of the inward current resembles the Na current recorded from squid axon in its rapid and voltage-dependent activation kinetics (time to peak, ~2.3 [−30 mV], 1.9 [−10 mV], and 1.7 ms [+10 mV] at 10°C), as well as in its characteristic inactivation and TTX sensitivity.

The Ca Current

A typical set of membrane currents obtained from a cell bathed in ASW with TTX (200 nM) is presented in Fig. 5. Step depolarizations from a holding potential of −100 mV to the indicated voltages activate inward currents that follow, after an initial delay, an approximately exponential time course with time constants ranging from 5 ms for a depolarization to −30 mV to 1.5 ms for a depolarization to +10 mV. These currents were maintained during the 15-ms

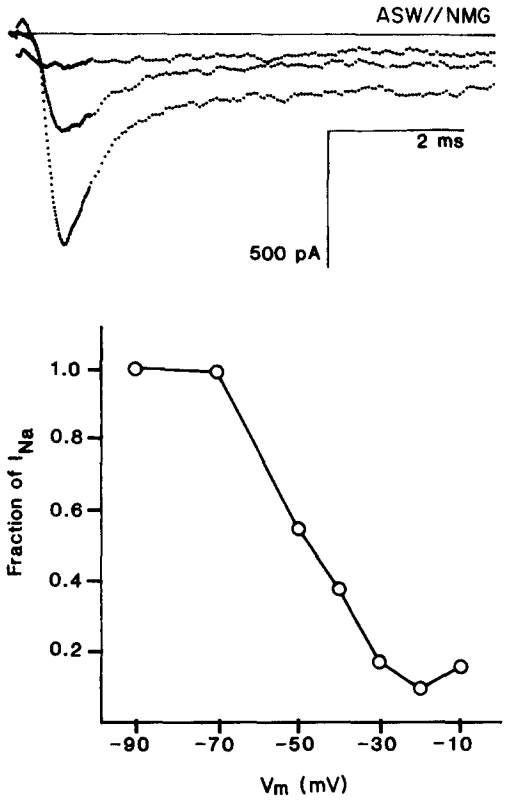

FIGURE 4. Na current inactivation. (*A*) Currents elicited by a test pulse to 0 mV after 25-ms prepulses to −70, −50, and −30 mV. Holding potential, −70 mV. (*B*) Voltage dependence of the steady state inactivation of I_{Na}. The value of the peak inward current, normalized relative to the peak value at −90 mV, is plotted against the membrane potential during the prepulse. The curve was drawn by eye.

pulses and were followed by inward current tails upon the return to the holding potential. The magnitude of the current during the pulse increased with membrane potential, reaching its peak at 0 mV, and then decreased, approaching the zero-current level at +40 mV (see Fig. 6*A*). That this inward current is carried by Ca^{2+} is strongly suggested by two experimental results. (*a*) Pulse and tail inward currents with the same general properties as those described were recorded from cells bathed in an external solution in which all of the permeant

cations except Ca^{2+} were replaced by the impermeant cation Tris. In this situation, Ca^{2+} is the only plausible carrier for the inward current. (*b*) The peak magnitude of the inward current recorded in Tris solutions with 50 mM Ca^{2+} was ~1.5 times larger than that obtained from cells bathed in a Tris solution with 10 mM Ca^{2+}.

An inspection of the currents obtained upon the return to the holding potential after step depolarizations such as those shown in Fig. 5 reveals that the tail current did not decay with a single-exponential time course, but rather as the sum of two kinetically distinct components. Fits of two exponentials to the tail currents, using a stripping procedure, were performed in order to estimate the deactivation time constants as well as the relative amplitudes of both components

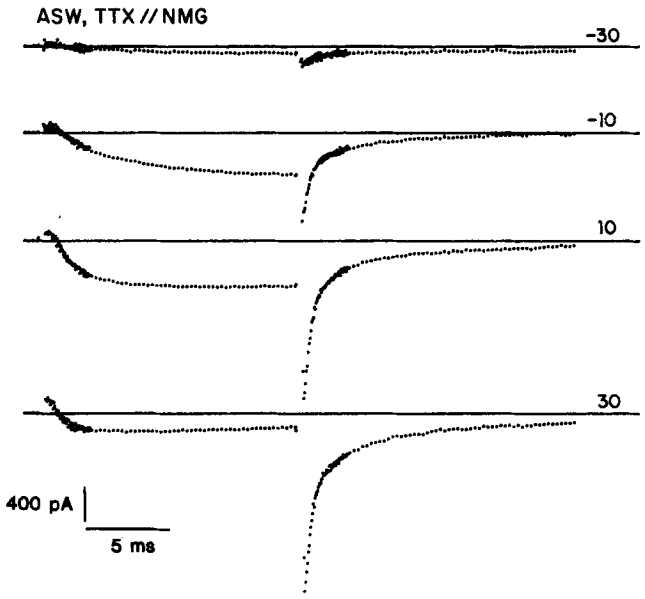

FIGURE 5. The Ca current. Inward currents recorded in the presence of 200 nM TTX in the bathing medium. Holding potential, −90 mV; values of 15-ms depolarizations are indicated on each trace.

under different experimental conditions. In the descriptions that follow, tail amplitudes have been obtained by this exponential-fitting procedure, and have been extrapolated to the initial time of repolarization. In seven cells studied, the tail currents could be accurately fitted by the sum of two exponentials with time constants of 4.05 ± 0.28 (mean ± standard deviation) and 0.27 ± 0.04 ms for repolarizations to −100 mV. Following the nomenclature used by Armstrong and Matteson (1985), we will refer to these two components of the tail current as SD (slow deactivating) and FD (fast deactivating), respectively.

It is suggested by records such as those in Fig. 5 that for relatively small depolarizations, the tail current is composed almost exclusively of the SD component, whereas the FD component becomes evident only at higher depolariza-

tions. Their relative voltage dependence was examined by applying 20-ms depolarizations to various potentials and recording the inward current upon the return to the holding potential. Fig. 6*B* shows a plot of the normalized SD and FD tail amplitudes as a function of the membrane potential during the preceding

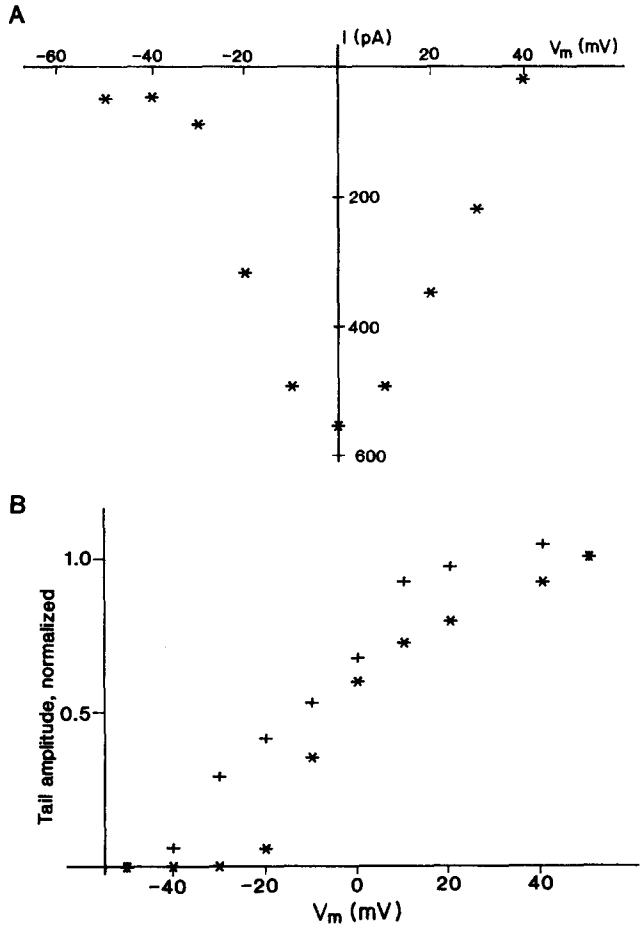

FIGURE 6. (*A*) Current-voltage relation for the Ca current: the peak magnitude of the inward current is plotted as a function of membrane potential. (*B*) Voltage dependence of the two tail components. SD (+) and FD (*) tail amplitudes, determined by fitting two exponentials, have been normalized to their value after a pulse to 50 mV and plotted against the activating membrane potential. For both *A* and *B*, data are from the cell shown in Fig. 5. 200 nM TTX was added to the external solution for the experiments presented in this and the following figures.

pulse. It confirms the suggestion that the SD component of the inward tail current activates at more negative potentials than the FD component.

These two components of the Ca current differ also in their activation time course. Fig. 7*A* presents the tail currents obtained after 2- and 10-ms depolari-

zations to 0 mV. In the 10-ms trace, two kinetic components of the tail current can be clearly distinguished, with time constants of 3.81 and 0.23 ms; the solid line in this trace corresponds to the exponential fit for the slow component of the tail. This component is not present after a brief 2-ms depolarization, in which case the tail can be fitted by a single exponential with a time constant of 0.25 ms. Fig. 7*B* shows the plot of normalized tail amplitudes, obtained from exponential fits, as a function of the duration of the activating pulse, averaged from

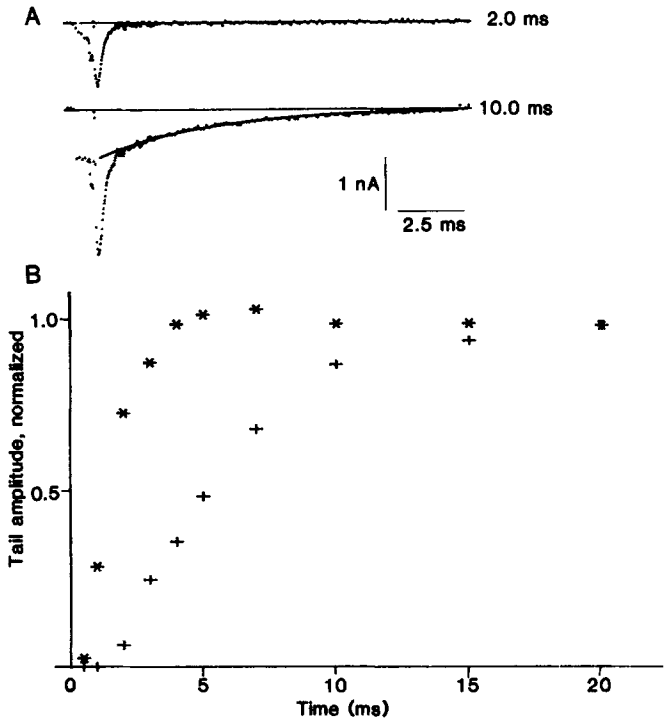

FIGURE 7. Activation kinetics for the SD and FD tail components. (*A*) Tail currents obtained upon the return to −100 mV after 2- and 10-ms depolarizations to 0 mV. The initial portion of both traces includes a few points of baseline, taken before the activating pulse, and the last 1.0 ms of current during the activating pulse. (*B*) The amplitudes of the FD (*) and SD (+) components, determined by fitting two exponentials, have been normalized to their value at 20 ms and are plotted as a function of the duration of the activating pulse. Data are averages from six different cells.

six different cells. From these results, it is evident that the FD component activated more rapidly, reaching its peak value in ~5–7 ms. The activation of the SD component proceeded with a slower time course, approaching its peak value by 20 ms.

The degree to which Ca currents inactivate varies widely among different preparations, and recent studies both at the macroscopic level (e.g., Armstrong and Matteson, 1985) and at the single channel level (e.g., Nowycky et al., 1985)

indicate that various types of Ca channels differ with respect to their inactivation properties. Under our experimental conditions, the total Ca current showed a very small decline during long depolarizations (Fig. 8*C*) and depolarizing prepulses of up to 300 ms in duration had very little effect on the current amplitude during a subsequent test pulse. This suggests that either the channels responsible

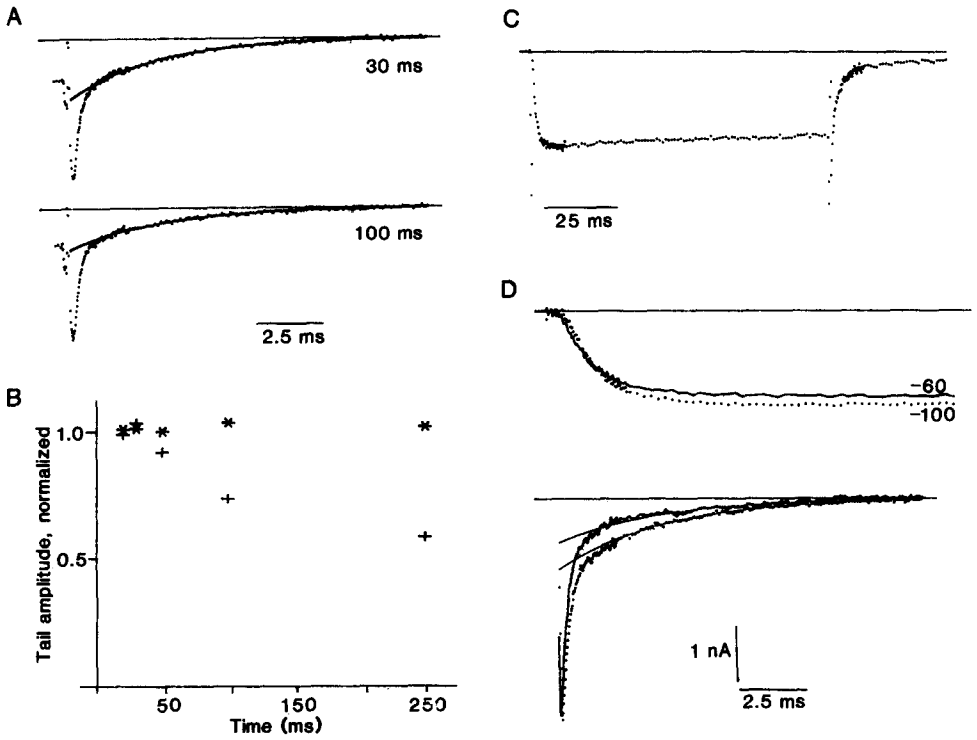

FIGURE 8. Inactivation properties of the two tail components. (*A*) Tail currents recorded after pulses to 0 mV for the indicated durations. The solid line on each trace corresponds to the exponential fit for the slow component. The initial portion of both experimental traces corresponds to a few points of baseline, taken before the activating pulse, and the last 1.0 ms of the activating pulse. (*B*) Normalized SD (+) and FD (*) tail amplitudes, determined by a two-exponential fitting, are plotted against the pulse duration. (*C*) Current recorded during a 100-ms depolarization to 0 mV. (*D*) Effect of changing the holding potential on both pulse current and tail current. See text for details. The 1-nA calibration bar applies to all current traces. The data in *A* and *B* are from the same cell; those in *C* and *D* from two different cells.

for this current do not inactivate significantly or an inactivating component contributes a relatively small fraction of the current during the pulse. An analysis of the tail currents indicates that the SD component does in fact inactivate, although the extent of inactivation is smaller in this preparation than in GH3 cells, for example, where it is complete (Matteson and Armstrong, 1986). Fig.

8*A* shows the tail currents recorded after 30- and 100-ms depolarizations to 0 mV; the solid line on each trace corresponds to the exponential fit for the SD component. In this case, the FD component of the tail had basically the same amplitude after 30- and 100-ms pulses (3.41 nA, $\tau = 0.23$ ms; 3.26 nA, $\tau = 0.24$ ms, respectively; amplitude values were extrapolated to the initial time of repolarization). In contrast, the extrapolated amplitude of the SD component decreased from 1.14 nA at 30 ms ($\tau = 3.09$ ms) to 0.816 nA at 100 ms ($\tau = 3.06$ ms). The plot in Fig. 8*B* presents the normalized tail amplitudes for FD and SD components of the tail obtained after depolarizations of increasing duration. Pulses of up to 250 ms in duration did not affect the amplitude of the subsequent FD tail component, but led to a decline in the SD component, which decreased to 63% of its peak value after a 250-ms pulse.

The effect of varying the holding potential on the pulse current, as well as both tail components, is illustrated in Fig. 8*D*. The upper traces show currents recorded during 15-ms depolarizations to 0 mV from a holding potential of −100 (dotted trace) and −60 mV (solid trace). In the latter case, the current was slightly reduced, its amplitude being 90% of the value obtained from a holding potential of −100 mV. The lower traces show the tail currents under these two conditions, obtained upon repolarization to −100 mV (HP = −100 [dotted trace] and −60 mV [solid trace]). The continuous line on each trace corresponds to the fit for the SD component. Although the FD component of the tail was not affected by the change in holding potential, the SD component decreased by 40%. This relatively large decline in the amplitude of the SD component as compared with the small decline in pulse current suggests that, as is the case in GH3 cells, a larger fraction of the pulse current was carried by FD-type channels than by SD-type channels. Thus, although the latter inactivated during maintained depolarizations, the current during the test pulse does not reflect this inactivation process as clearly as the tail currents do.

The two components of the Ca tail current also differ in their sensitivities to block by external divalent cations. Cd^{2+}, at concentrations between 1 and 5 mM (in the presence of 10 mM Ca^{2+}), abolishes all of the Ca current, an effect that is not completely reversible after cells have been exposed to this inorganic blocker for >10–15 min. Preliminary experiments using lower concentrations of Cd^{2+} (10–100 μM) led to a significant (>60%) reduction of the pulse current and of the FD component of the tail current but had less effect on the SD component of the tail current. This is in agreement with the results obtained in guinea pig ventricular cells (Nilius et al., 1985), where, at the single channel level, the lower-threshold, inactivating channel (T-type of Ca channel in their nomenclature) was shown to be less sensitive to external Cd^{2+} than the higher-threshold, noninactivating channel (L-type of Ca channel).

K Currents

As mentioned earlier, the predominant ionic current in this preparation is outward and is carried by K^+. The remainder of this section is concerned with a description of the properties of this current, as studied in both the whole cell and the isolated patch configuration.

Fig. 9*A* shows the currents recorded from a cell bathed in ASW with 200 nM TTX and 1 mM Cd^{2+} in order to eliminate the inward currents, and perfused with a K-containing solution (KFG, Table I). When the membrane potential was held at −90 mV and 20-ms depolarizing pulses were applied, the outward

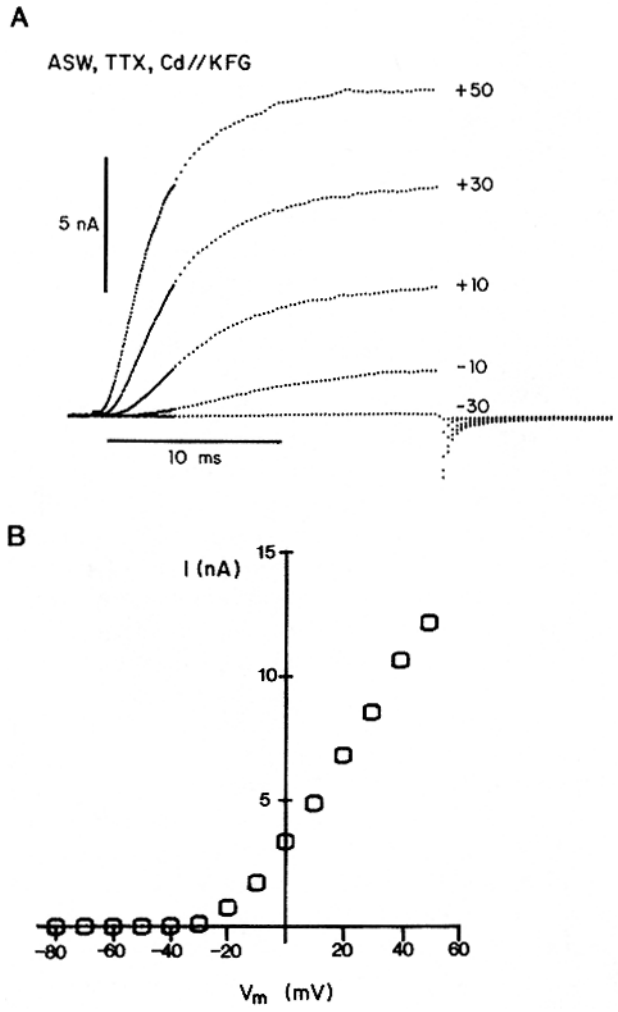

FIGURE 9. The K current. (*A*) Outward currents, recorded in ASW with 200 nM TTX and 1 mM $CdCl_2$. Internal solution, KFG. Holding potential, −90 mV. Depolarizing steps to the values indicated on each trace. (*B*) Isochronal current-voltage relation. Current magnitude at the end of a 20-ms pulse is plotted against the membrane potential.

currents recorded resembled those obtained from squid giant axon in their voltage dependence and sigmoid activation time course. The time to reach 50% of the peak value was strongly voltage dependent, ranging from 10 ms at −20 mV to 3 ms at +50 mV. The isochronal current-voltage relation, obtained by

plotting the current at the end of 20-ms depolarizations vs. the membrane potential, is shown in Fig. 9*B*. This K current has an activation threshold at approximately −20 to −30 mV.

When studied with longer depolarizations, these currents showed a significant decline, as shown in Fig. 10*A*. When 250-ms depolarizations were applied from a holding potential of −90 mV to values ranging from −20 to +60 mV, the outward current decayed to 35–40% of its peak value by the end of the pulse. The extent of inactivation, as calculated by the fraction of peak current remaining at the end of the pulse, does not depend on the membrane potential.

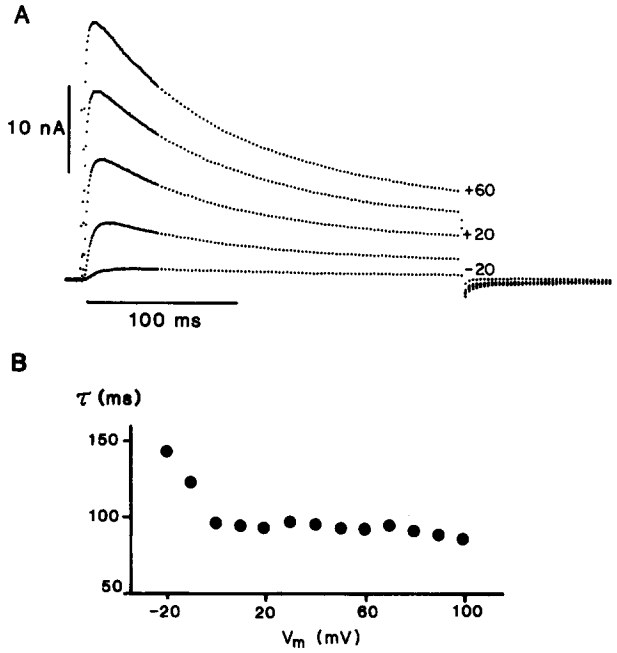

FIGURE 10. Outward current decay. (*A*) Current elicited by 250-ms depolarizations from a holding potential of −90 mV. (*B*) Time constants of decay as a function of membrane potential. The estimates of the time constant were obtained by fitting a single exponential to the decaying phase of the outward currents recorded with 250-ms pulses.

Estimates of the time constant of decay, obtained by fitting a single exponential to the falling phase of the current, are presented in Fig. 10*B*. The estimated time constants are of the order of 80–100 ms and show little voltage dependence for depolarizations to values >0 mV. For smaller depolarizations, the fits are less accurate, because of the smaller current size; furthermore, the slower activation kinetics may influence the estimated time constant of decay in that voltage range.

In order to elucidate whether the decline of this current with prolonged depolarizations was the result of external K ion accumulation during the pulse or of a change in conductance with time, instantaneous current-voltage relations were obtained for pulses of various durations. The results of these experiments

are illustrated in Fig. 11. The two traces in Fig. 11*A* show the last 3 ms of the current recorded during 20-ms (upper trace) and 250-ms (lower trace) depolarizations to +40 mV, and the tail currents obtained upon the return to the holding

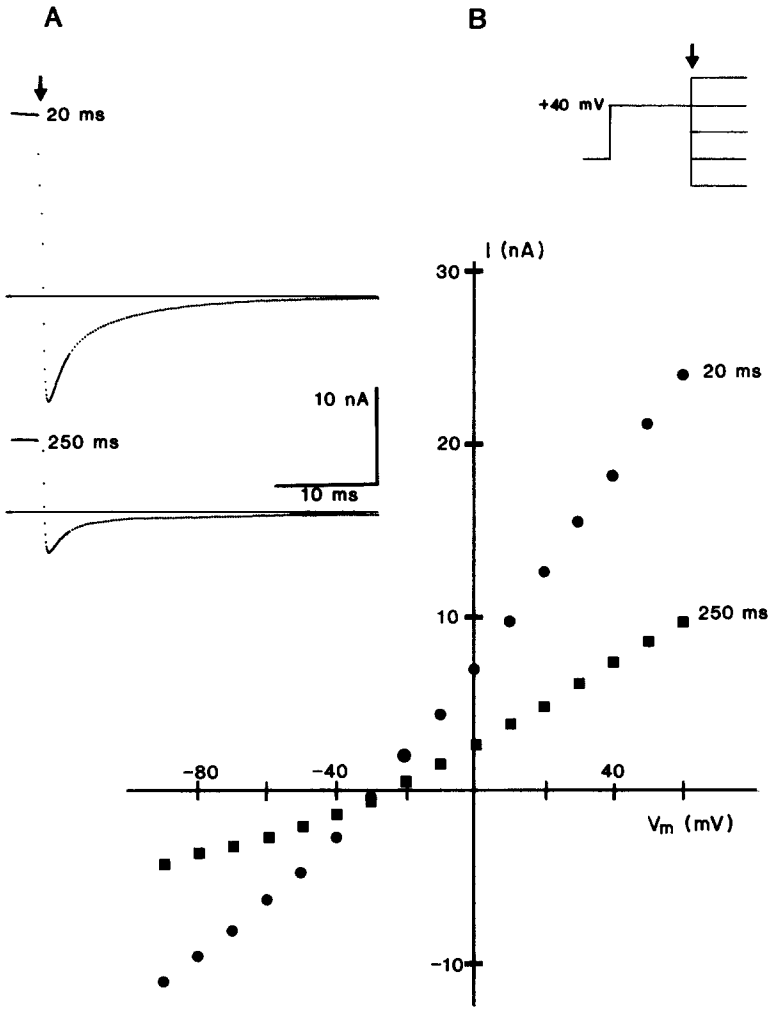

FIGURE 11. Evidence of K conductance inactivation. (*A*) Tail currents recorded at the holding potential (−90 mV) after 20- and 250-ms depolarizations to 40 mV. (*B*) Instantaneous current-voltage relation. The inset illustrates the protocol used. After depolarizations to 40 mV, the membrane potential was stepped to various levels; the initial amplitude of the tail current is plotted against the membrane potential. The circles correspond to the values obtained after 20-ms depolarizations; the squares correspond to those obtained after 250-ms depolarizations.

potential (−90 mV). These measurements were made in the presence of 50 mM external K^+ to minimize any accumulation artifacts. It is clear that both the current level at the end of the pulse and the initial tail amplitude are much larger for the 20-ms depolarization. The decrease in tail amplitude at 250 ms argues

against significant accumulation effects being responsible for the decline of the current. Further evidence on this point was obtained from studies of instantaneous current-voltage (*I-V*) relations measured after short (20 ms) and long (250 ms) pulses (Fig. 11*B*). These were obtained by stepping from −90 mV to +40 mV for 20 or 250 ms and returning to a different potential, as indicated in the inset. The initial amplitude of the tail current is plotted against the final level of membrane potential. The equilibrium potential of the outward current, obtained from the intersection of the curves with the voltage axis, shows a small change

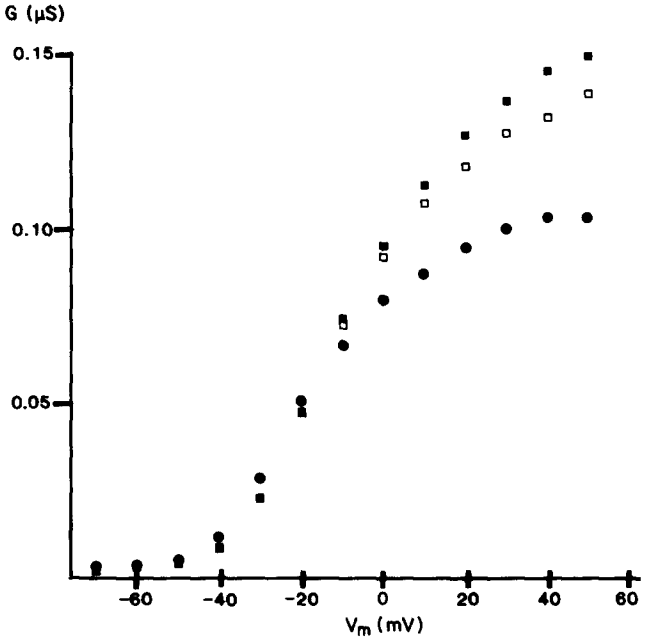

FIGURE 12. Conductance-voltage relations obtained at 10 (■), 20 (□), and 50 (●) ms. The conductance values at each potential were calculated as $G = (I_e - I_t)/(V - V_H)$, where I_e is the current at the end of the pulse, I_t is the initial current amplitude after return to the holding potential, V is the membrane potential during the pulse, and V_H is the holding potential.

with longer depolarizations, which was −30 mV at 20 ms and −23 mV at 250 ms. This small change in E_K could be caused by an increase in external K^+ (from 50 to 66 mM) resulting from accumulation on the external side of the membrane, but it is insufficient to account for the observed 65% decline in the current level. A decline in K conductance is confirmed by estimates of the slope conductance from the linear part of the instantaneous *I-V* curves in Fig. 11*B*. The conductance at 250 ms is 40% of its value at 20 ms. The same type of data were obtained from cells bathed in a variety of external K^+ concentrations, at times ranging from 5 to 250 ms after the beginning of the activating pulse. All the data are consistent with a decrease in outward conductance being the principal cause for the observed decline in the current during prolonged depolarizations.

Conductance-voltage relations obtained at 10, 20, and 50 ms are shown in Fig. 12. The conductance, for large depolarizations, was maximal at 10 ms and

decreased with time, which reflects the inactivation process. For smaller depolarizations, the conductance peaked at later times, reflecting the voltage dependence of activation gating. The midpoint of the *g-V* curve is approximately −15 mV for the 50-ms pulses.

The voltage dependence of the steady state level of K channel inactivation was studied by varying the holding potential and recording the currents in response to depolarizing pulses. Fig. 13*A* illustrates the results obtained at holding potentials of −90 and −30 mV. The peak current at a given potential was strongly

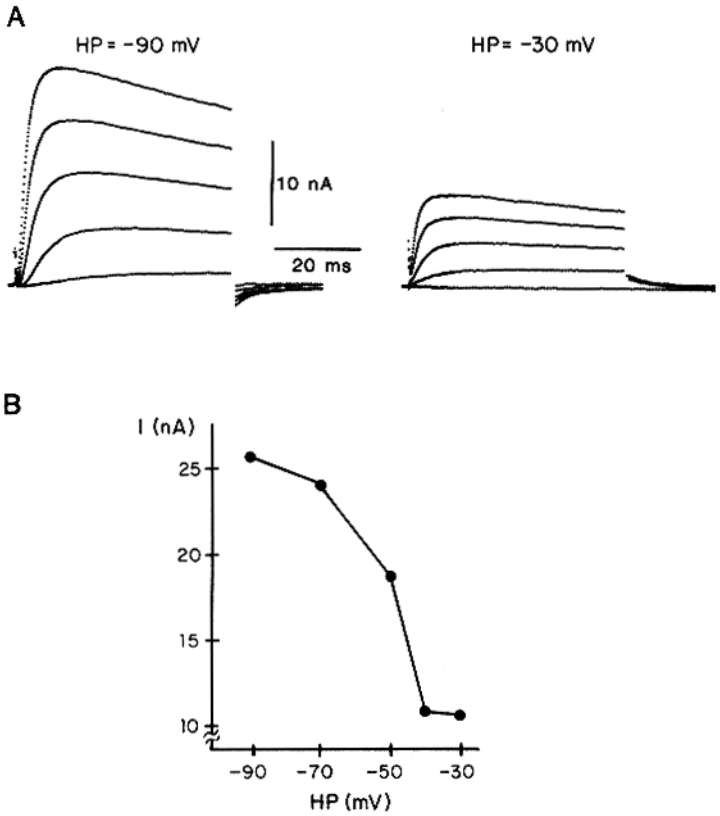

FIGURE 13. Steady state properties of the I_K inactivation. (*A*) I_K recorded for depolarizations to −30, −10, 10, 30, and 50 mV from holding potentials of −90 (left) and −30 (right) mV. (*B*) Peak outward current elicited by a 50-ms pulse to 50 mV, plotted as a function of the holding potential. The curve was drawn by eye.

decreased by holding at a more depolarized potential. However, the activation kinetics appeared to be unchanged, since the time to reach 50% of the peak current value at a given potential did not depend on the holding potential. A steady state inactivation curve for this current is presented in Fig. 13*B*, where the peak current measured for an activating pulse to +50 mV is plotted as a function of the holding potential. This curve has a midpoint of −47 mV; the noninactivating fraction of the current fell to ~40% at −30 mV, where the curve reaches its steady state level.

To study the properties of this conductance at the single channel level, we performed experiments on excised outside-out patches, using the same ionic conditions as those in whole cell mode. Under these conditions, most patches had a large density of K channels, and ensemble fluctuation analysis (Sigworth,

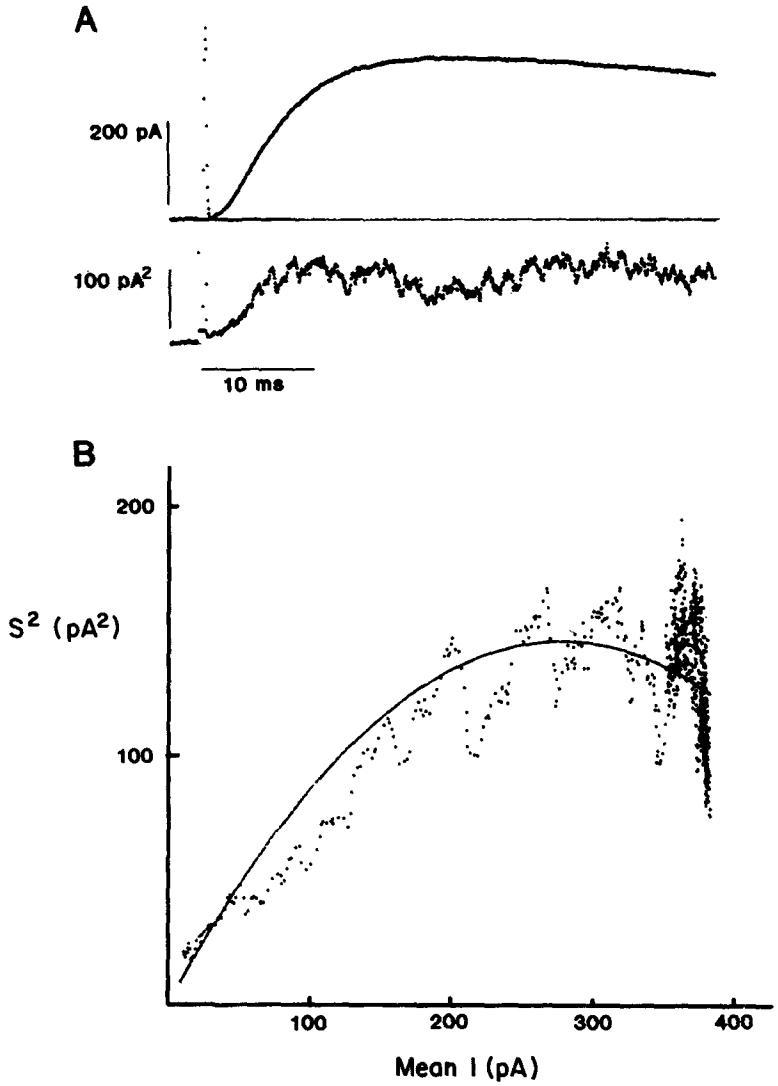

FIGURE 14. Ensemble analysis of the K current from excised outside-out patches. (*A*) Time course of the mean current (top trace) and variance (lower trace) calculated from 40 depolarizations to −10 mV. (*B*) Plot of the variance as a function of the mean current. See text for details.

1980) was performed to obtain an estimate of the value of single channel conductance for the channels responsible for this inactivating K current.

Fig. 14*A* shows the mean current calculated from a set of 40 depolarizations to −10 mV, and the associated ensemble variance. The maximum variance for

this set of records was 196 pA^2, which corresponds to ~2.5% of the peak mean current. A plot of the variance as a function of the mean current is shown in Fig. 14 *B*. The data points are represented by dots. The solid line corresponds to that predicted by the quadratic equation derived from a two-conductance-state theory for the gating of independent, identical channels (Sigworth, 1980) with the values of the single channel current (i) and the number of channels (N) given in the panel. Both the single channel current (i) and the number of channels (N) were free parameters in the fit. The value of single channel conductance (γ), calculated as $\gamma = i/(V - V_K)$, was 16 pS.

The estimates of i, N, and γ obtained from several experiments are presented in Table II. In experiment 1, the holding potential was set at −40 mV, whereas

TABLE II

Conductance Estimates from Ensemble Analysis

	V_m	N	γ
	mV		*pS*
Experiment 1	−10	294	12.4
	10	428	12.1
	30	400	15.1
Experiment 2	−20	380	13.3
	20	598	14.7
Experiment 3	−30	583	11.6
	−20	644	12.3
	−10	575	17.4
Experiment 4	−10	68	11.4
	20	164	9.4
	50	135	12.2
Experiment 5	−10	519	16.3
			Mean = 13.3
			SD = 2.2

Values of single channel conductance (γ) and number of channels (N) obtained from five different experiments. The holding potential was −40 mV in experiment 1, −70 mV in all others. See text for details.

in the rest the holding potential was −70 mV. Estimates of γ are independent of holding potential and of the pulse potential; furthermore, the values for N did not change significantly with membrane potential. The agreement between the experimental results and the predictions made by the two-state theory suggests that the majority of the outward current being recorded under our experimental conditions is the result of the activation of a single population of identical and independent channels.

Recently, we have been able to obtain recordings of the current flowing through single K channels in excised outside-out patches. Fig. 15*A* shows some typical records obtained with a pipette containing 530 mM K^+. The patch was maintained at −60 mV and 100-ms pulses to 0 mV were applied. Under these

conditions, outward current steps can be easily discerned, the amplitude at this potential being ~1.3 pA, which corresponds to a single channel conductance of 22 pS. The averaged current obtained from 20 individual records is presented below. Its kinetics resemble those of the macroscopic K current described here

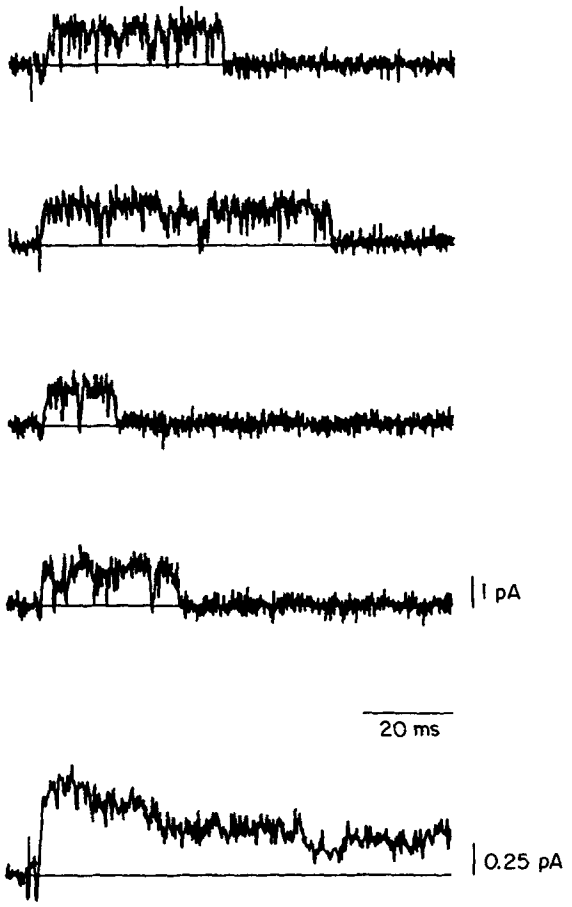

FIGURE 15. Single K channels recorded from an excised outside-out patch. The internal solution contained 530 mM K^+ and the outside of the patch was bathed in ASW. (*A*) Selected records from a series of currents elicited by 100-ms depolarizations to 0 mV from a holding potential of −60 mV. Subtraction for leak was applied and the records were digitally filtered at 2.5 kHz. (*B*) Average of 20 consecutive current traces at the same potential.

in both its activation and inactivation time course. These preliminary results further suggest that the inactivating outward current described in this work results from the activation of a single type of voltage-dependent K channel. A more detailed description of the properties of this K conductance at the single channel level will be presented in another publication.

DISCUSSION

The GFL Neuron Preparation

The GFL neurons should be useful in addressing a number of questions. The dissociated tissue from a single lobe contains numerous cell bodies with and without axonal processes. Those healthy cells with processes are routinely seen to grow in culture and send out growth cones and microspikes. This observation raises the possibility of using this system to study the mechanisms underlying axo-axonal recognition and fusion. Of more direct interest to the study of ionic channels is the possibility of investigating in this preparation the regulatory processes that control the synthesis and insertion of channel proteins in the different regions of a neuronal cell. Although no conclusive evidence is available as to the subcellular localization of channel synthesis in the giant axon system, it is likely that, as is the case for many membrane-associated proteins, these molecules are synthesized in the cell body and then move by axoplasmic transport down the axon to be inserted in specified locations. In this case, the GFL preparation could be used as the source of the genetic material responsible not only for the structural formation of the giant axon, but also for the synthesis and control of the spatial distribution of various channel types. Finally, recent developments in microscale cloning techniques may make possible the cloning of the squid axonal Na and K channels from a relatively small amount of material extracted from the cell bodies.

The Voltage-dependent Ionic Currents

The Na current. Axon-free cell bodies have a large outward current and at least two discernible inward currents. One of these inward currents seems to be the same as the Na conductance from the giant axon as judged by its voltage-dependent activation and inactivation and its TTX sensitivity. However, its magnitude, although variable, is small in most cells (maximum current densities of the order of 6 $\mu A/cm^2$). We selected cells that were round and free of axonal stumps, but it is possible that a portion of the axonal membrane may retract into the cell and contaminate the somatic currents, which with perfect separation might be free of I_{Na}. In any case, this paucity of somatic Na currents contrasts with the axon, where peak Na current densities are of the order of 3 mA/cm^2 under similar ionic conditions. This implies that GFL neurons have a mechanism for selectively inserting Na channels at the appropriate site and excluding them from the somatic membrane. However, we cannot rule out the possibility that the Na channels are present but not functional in the GFL cells.

The Ca current. The inward current remaining after TTX has been identified as being carried through Ca channels. A voltage-dependent, TTX-insensitive inward Ca current has been previously recorded from internally perfused and from dialyzed squid giant axons (DiPolo et al., 1983). The current-voltage relation for the axonal Ca current closely resembles that of the somatic current. Furthermore, like the somatic current, the axonal Ca current does not inactivate during step depolarizations of up to 70 ms in duration, although it does decline during steady state depolarizations. Regarding relative current densities, axonal Ca currents recorded in the presence of 8 mM external Ca^{2+} by DiPolo et al.

were of the order of 1 $\mu A/cm^2$, whereas the peak Ca currents in the cell bodies (in 10 mM Ca^{2+}) were in the range of 10–30 $\mu A/cm^2$; this is a relatively small difference when compared with the large regional difference in Na channel distribution. There is no detailed analysis of the time course of tail current in the axon which can be compared with our observations regarding two kinetically distinct components of the somatic Ca current. It would be of interest to explore the axonal Ca currents to elucidate further whether the two types of channels that are suggested by our present results are also functional in the axon.

Ca currents have been studied in another squid cell, the presynaptic element of the giant synapse preparation (Llinas et al., 1981; Charlton et al., 1982; Augustine and Eckert, 1984; Augustine et al., 1985). It is worth recalling that the GFL cells are responsible for the formation and maintenance of the giant axon, the proximal-most portion of which forms the postsynaptic side of the giant synapse (Young, 1939). The comparison of "pre-" and "postsynaptic" Ca currents is therefore of uncertain value, but it is nonetheless interesting to note that they have common features. Thus, as is the case for the GFL Ca currents, the *I-V* relation in the presynaptic current has a threshold at about −40 mV, peaks between −10 and 0 mV, and has similar activation kinetics (taking into account the slightly higher temperature of Llinas et al., 1981), and the current during the pulse shows little or no inactivation. With respect to the time course of deactivation, Llinas et al. (1981) found that the tail currents could be described as "close to a single exponential" with time constants in the range of 0.42–0.67 ms. Augustine et al. (1985) stated that the tail currents decayed with two or more exponential components. An examination of their records (cf. Figs. 8 and 9) shows clearly that for larger depolarizations, a fast component dominates that is complete in ~2.0 ms. Considering the differences in the closing voltages used (−70 mV in the studies of both Llinas et al. and Augustine et al., and −100 mV in the present study), our fast component (τ = 0.27 ms at −100 mV) is similar to the major component of their records. It remains to be seen whether, under appropriate experimental conditions, a component of the Ca tails with slow deactivation kinetics can be observed in the presynaptic terminal.

Several experimental results suggest that there are two Ca channel types in GFL neurons. It is important to emphasize that the interpretation of our results in terms of two channel types relies on the analysis of the properties of the Ca current tails originally used by Armstrong and Matteson (1985). Thus, it is useful to summarize our observations on these properties. Small depolarizations from a holding potential of −100 mV lead to small, slowly activating currents during a 20-ms pulse and a slow inward tail current upon returning to the holding potential. As the pulse amplitude increases, the current increases up to ~0 mV and the kinetics of the tail current become more complicated as a distinct fast component comes to dominate. If the pulse duration is very short (2 ms), then a large pulse elicits only a fast tail current. The slow component of the tail current clearly develops later. As the pulse duration is increased further, this slow component increases, reaching a maximum at ~25 ms, and then decreases as the pulses are lengthened out to 250 ms. Increasing the extent of steady state inactivation by holding the cell at −60 mV leads to a slightly smaller current during the pulse and a decrease in the magnitude of the slow component of the

tail current. The magnitude of the fast component of the tail is essentially insensitive to holding potential and pulse duration for pulses longer than 10 ms.

A simple linear sequential scheme for a channel with several closed states (e.g., FitzHugh, 1965) can produce multiple exponential tail components, provided that at least the last forward rate constant and two of the closing rate constants are nonzero at the voltage range where closings are measured (−100 mV in these experiments). However, this would predict that channel openings would occur at potentials well below what we observe experimentally (see Fig. 6*A*). Furthermore, fast closing kinetics are predicted by this scheme at all activating voltages, but we found no fast component to the Ca tail for depolarizations below −20 mV (see Fig. 6*B*). The differences in the degree of inactivation of both components are also difficult to explain with a simple linear scheme. Although more complicated kinetic schemes could explain the results summarized above, in view of the increasing amount of evidence for a multiplicity of Ca channel types in a variety of preparations, it seems to us that the simplest interpretation of these observations is that there are two kinetically distinct types of Ca channels, as has been proposed in similar studies on GH3 cells. In the case of GH3 cells (Matteson and Armstrong, 1986), the SD component inactivates completely, and thus by using long voltage-clamp pulses, the FD component could be studied in isolation. This is not the case for the GFL neurons, where the SD component only inactivates by ~40%. However, we can study the FD component alone by using brief pulses (see Fig. 7) and the SD component by using small depolarizations (Fig. 6).

There is ample support in the literature, from the analysis of both macroscopic and single channel Ca currents, as well as voltage recording, for the idea that there are two or more components to the Ca conductance and that they activate at different thresholds (Hagiwara et al., 1975; Llinas and Yarom, 1981; Fox and Krasne, 1984; Carbone and Lux, 1984*a*, *b*; Matteson and Armstrong, 1984*b*, 1986; Armstrong and Matteson, 1985; Nowycky et al., 1985; Fedulova et al., 1985). All of these reports agree, as we do, that the low-threshold component inactivates more completely than the high-threshold component. However, since most of these reports do not analyze deactivation kinetics, a precise comparison of the properties of the various channel types reported with our results cannot easily be made at this point.

The K current. The present study indicates that the outward current of GFL neurons results from the activation of a single type of voltage-dependent K channel. In contrast to many other preparations, there seems to be no significant Ca-activated K conductance in these cells, since the same type of macroscopic behavior is recorded in cells perfused with or without Ca chelators (EGTA and fluoride). Fluctuation analysis of currents recorded from excised outside-out patches with a high density of channels, as well as direct observations of single channel events, are consistent with a single type of K channel being responsible for the inactivating K current. Estimates of the single channel conductance from fluctuation analysis were of the order of 13 pS, whereas direct measurements of single channel current amplitudes yielded a value of 20 pS. This difference is probably accounted for by the higher concentration of intracellular K^+ used with

the single channels than in the fluctuation analysis study (530 and 295 mM, respectively). These results are consistent with a recent study at the single channel level (Standen et al., 1985), which has demonstrated that the inactivating K current in skeletal muscle sarcolemma, originally described by Adrian et al. (1970), results from the activation of a single type of K channel having a unitary conductance of ~15 pS.

The macroscopic K currents of GFL neurons resemble those present in the axon in their activation time course and voltage dependence. Pharmacologically, they share with the axonal current (Armstrong and Binstock, 1965) their sensitivity to block by internal but not external TEA. These currents decline during maintained depolarizations, as the result of a decrease in K conductance that takes place with a time constant of the order of 80 ms. In this respect, the GFL I_K is qualitatively similar to the inactivating K current that was originally described for neuronal cells in studies of the supramedullary neurons of puffer fish (Nakajima and Kusano, 1966; Nakajima, 1966) and which has been found in a variety of neuronal and non-neuronal cells.

With respect to its inactivation, the somatic K current may differ from the axonal current in that the latter has been found to inactivate with a much slower time course, i.e., on the order of seconds (Ehrenstein and Gilbert, 1966; Chabala, 1984). We have no evidence to relate this slow inactivation with the faster process that we have demonstrated in the cell bodies. It is possible that there is an inactivation process in the axon that proceeds with time constants in the 100-ms range, but its presence may be difficult to detect because of the changing driving forces that result from the accumulation and depletion of K ions. Usually, this and other technical considerations such as electrode polarization have discouraged voltage-clamp experiments in which long pulses with large current flow are applied to the squid axon. A detailed comparison of the results obtained at the single channel level in both the axon (Conti and Neher, 1980; Llano and Bezanilla, 1985) and in the cell bodies (Llano et al., 1986) will be useful for a better understanding of the qualitative and quantitative differences between somatic and axonal K channels.

We thank Dr. Clay M. Armstrong for his constant support and invaluable discussions throughout the course of this study. It has been a privilege to work in his laboratory.
This work was supported by National Institutes of Health grant 1R01 NS12547 to Dr. C. M. Armstrong and a Muscular Dystrophy Association postdoctoral fellowship to I. Llano.

Original version received 17 December 1985 and accepted version received 10 April 1986.

REFERENCES

Adrian, R. H., W. K. Chandler, and A. L. Hodgkin. 1970. Slow changes in potassium permeability in skeletal muscle. *Journal of Physiology.* 208:645–668.

Armstrong, C. M., and F. Bezanilla. 1974. Charge movement associated with the opening and closing of the activation gates of the Na channel. *Journal of General Physiology.* 63:533–552.

Armstrong, C. M., and L. Binstock. 1965. Anomalous rectification in the squid giant axon injected with tetraethylammonium chloride. *Journal of General Physiology.* 48:859–872.

Armstrong, C. M., and D. R. Matteson. 1985. Two distinct populations of calcium channels in a clonal line of pituitary cells. *Science.* 227:65–67.

Augustine, G., M. P. Charlton, and S. J. Smith. 1985. Calcium entry into voltage-clamped presynaptic terminals of squid. *Journal of Physiology.* 367:143–162.

Augustine, G., and R. Eckert. 1984. Divalent cations differentially support transmitter release at the squid giant synapse. *Journal of Physiology.* 346:257–271.

Bookman, R. J., I. Llano, and C. M. Armstrong. 1985. Ionic currents from giant fibre lobe neurons of the squid. *Biophysical Journal.* 47:222*a*. (Abstr.)

Carbone, E., and H. D. Lux. 1984*a*. A low voltage-activated, fully inactivating Ca channel in vertebrate sensory neurons. *Nature.* 310:501–502.

Carbone, E., and H. D. Lux. 1984*b*. A low voltage-activated calcium conductance in embryonic chick sensory neurons. *Biophysical Journal.* 46:413–418.

Chabala, L. D. 1984. The kinetics of recovery and development of potassium channel inactivation in perfused squid (*Loligo pealei*) giant axons. *Journal of Physiology.* 356:193–220.

Charlton, M. P., S. J. Smith, and R. S. Zucker. 1982. Role of pre-synaptic calcium ions and channels in synaptic facilitation and depression at the squid giant synapse. *Journal of Physiology.* 323:173–193.

Cole, K. S. 1949. Dynamic electrical characteristics of the squid axon membrane. *Archives de Sciences Physiologiques.* 3:253–258.

Conti, F., and E. Neher. 1980. Single channel recordings of K^+ currents in squid axons. *Nature.* 285:140–143.

Dagan, D., and I. B. Levitan. 1981. Isolated identified *Aplysia* neurons in cell culture. *Journal of Neuroscience.* 1:736–740.

DiPolo, R., C. Caputo, and F. Bezanilla. 1983. Voltage-dependent calcium channels in the squid axon. *Proceedings of the National Academy of Sciences.* 80:1743–1745.

Ehrenstein, G., and D. L. Gilbert. 1966. Slow changes of potassium permeability in the squid giant axon. *Biophysical Journal.* 6:553–566.

Fedulova, S. A., P. G. Kostyuk, and N. S. Veselovsky. 1985. Two types of calcium channels in the somatic membrane of new-born rat dorsal root ganglion neurones. *Journal of Physiology.* 359:431–446.

FitzHugh, R. 1965. A kinetic model of the conductance changes in nerve membrane. *Journal of Cellular and Comparative Physiology.* 66(Suppl. 2):111–118.

Fox, A. P., and S. Krasne. 1984. Two calcium currents in *Neanthes arenaceodentatus* egg cell membranes. *Journal of Physiology.* 356:491–505.

Hagiwara, S., H. Ozawa, and O. Sand. 1975. Voltage-clamp analysis of two inward current mechanisms in the egg cell membrane of a starfish. *Journal of General Physiology.* 65:617–644.

Hamill, O. P., A. Marty, E. Neher, B. Sakmann, and F. J. Sigworth. 1981. Improved patch-clamp techniques for high-resolution current recording from cell and cell-free membrane patches. *Pflügers Archiv.* 391:85–100.

Hodgkin, A. L., A. F. Huxley, and B. Katz. 1952. Measurement of current-voltage relations in the membrane of the giant axon of *Loligo*. *Journal of Physiology.* 116:424–428.

Llano, I., and F. Bezanilla. 1985. Two types of potassium channels in the cut-open squid giant axon. *Biophysical Journal.* 47:221*a*. (Abstr.)

Llano, I., and R. J. Bookman. 1985. The K^+ conductance of squid giant fibre lobe neurons. *Biophysical Journal.* 47:223*a*. (Abstr.)

Llano, I., and R. J. Bookman. 1986. Single K channels recorded from squid GFL neurons. *Biophysical Journal.* 49:216*a*. (Abstr.)

Llinas, R., I. Z. Steinberg and K. Walton. 1981. Presynaptic calcium currents in squid giant synapse. *Biophysical Journal.* 33:289–322.

Llinas, R., and Y. Yarom. 1981. Electrophysiology of mammalian inferior olivary neurons *in vitro.* Different types of voltage-dependent ionic conductances. *Journal of Physiology.* 315:549–567.

Marmont, G. 1949. Studies on the axon membrane. I. A new method. *Journal of Cellular and Comparative Physiology.* 34:351–382.

Matteson, D. R., and C. M. Armstrong. 1984*a*. Na and Ca channels in a transformed line of anterior pituitary cells. *Journal of General Physiology.* 83:371–394.

Matteson, D. R., and C. M. Armstrong. 1984*b*. Evidence for two types of Ca channels in GH3 cells. *Biophysical Journal.* 45:36*a*. (Abstr.)

Matteson, D. R., and C. M. Armstrong. 1986. Properties of two types of calcium channels in clonal pituitary cells. *Journal of General Physiology.* 87:161–182.

Miledi, R. 1967. Spontaneous synaptic potentials and quantal release of transmitter in the stellate ganglion of the squid. *Journal of Physiology.* 192:379–406.

Nakajima, S. 1966. Analysis of K inactivation and TEA action in supramedullary cells of puffer. *Journal of General Physiology.* 49:629–646.

Nakajima, S., and K. Kusano. 1966. Behavior of delayed current under voltage clamp in the supramedullary neurons of puffer. *Journal of General Physiology.* 49:613–628.

Nilius, B., P. Hess, J. B. Lansman, and R. W. Tsien. 1985. A novel type of cardiac calcium channel in ventricular cells. *Nature.* 316:443–446.

Nowycky, M. C., A. P. Fox, and R. W. Tsien. 1985. Three types of neuronal calcium channels with different calcium agonist sensitivity. *Nature.* 316:440–443.

Sigworth, F. J. 1980. The variance of sodium current fluctuations at the node of Ranvier. *Journal of Physiology.* 307:97–129.

Sigworth, F. J. 1983. Electronic design of the patch clamp. *In* Single Channel Recording, B. Sakmann and E. Neher, editors. Plenum Press, New York. 3–35.

Standen, N. B., P. R. Stanfield, and T. A. Ward. 1985. Properties of single potassium channels in vesicles formed from the sarcolemma of frog skeletal muscle. *Journal of Physiology.* 364:339–358.

Young, J. Z. 1939. Fused neurons and synaptic contacts in the giant nerve fibres of cephalopods. *Philosophical Transactions of the Royal Society of London, Series B.* 229:465–505.